Structural and electronic properties of poly(3-hexylthiophene) π-stacked crystals

Arnaud Maillard* and Alain Rochefort†

Département de Génie Physique et Regroupement Québécois sur les Matériaux de Pointe (RQMP), École Polytechnique de Montréal, Montréal, Québec, Canada H3C 3A7

(Received 1 December 2008; revised manuscript received 18 February 2009; published 19 March 2009)

First-principles density-functional theory (DFT) method has been used to investigate the structural and electronic properties of regioregular head-to-tail poly(3-hexylthiophene-2,5-diyl) (rrP3HT) crystal. Among the different configurations investigated for the rrP3HT crystal, the most stable is a staggered structure which is 875 meV/monomer more stable than isolated rrP3HT chains. Electronic properties of the rrP3HT crystal are strongly influenced by the magnitude of π-π interactions that can be described by structural organization parameters such as the interchain distance in the stacking direction. From a disordered to a tightly packed polymer crystal, the direct band gap significantly decreases by ~0.8 eV, while the dispersion of highest occupied molecular-orbital and lowest unoccupied molecular-orbital bands increase by 0.60 and 1.33 eV, respectively.

DOI: 10.1103/PhysRevB.79.115207 PACS number(s): 71.20.Rv, 61.66.Hq, 72.80.Le, 82.35.Cd

I. INTRODUCTION

Recent development in organic semiconductors has opened a new prolific and dynamic area for research, and for possible applications using conjugated polymer materials.[1] An improved understanding and a better control of organic semiconductors properties, combined with a fairly simple manipulation, a large-scale and a low-cost deposition from solution make conjugated polymer a promising choice for the building of electroactive devices such as transistors,[2,3] displays,[4,5] and solar cells.[6,7]

The poly(3-alkylthiophenes) (P3ATs) family of semiconducting π-conjugated polymer has generated a lot of interest since the material was efficiently used in high-performance organic field-effect transistors.[8] P3ATs consist of a rigid π-conjugated backbone and alkyl side chains that play an important role in the polymer solubility. These alkyl side chains are placed at position "3" to address the insolubility problem of polythiophenes and to facilitate the processing steps for the production of the devices. It was observed that P3ATs with a high degree of regioregularity have a tendency to self-assemble into microcrystalline domains that are primarily organized into a stacking of the polymer backbones.[9,10] The molecular level order of these tightly packed domains should facilitate an efficient two-dimensional charge transport within a single conjugated polymer backbone, and between the stacked backbones helped by π-π coupling. Such highly anisotropic transport was observed with regioregular poly(3-hexylthiophene-2,5-diyl) (rrP3HT) that exhibits mobility up to about 0.1 $cm^2/V\,s$.[8]

Considering the importance of such microstructure in rrP3ATs films, numerous x-ray diffraction[9–11] and selected area electron diffraction[12] experiments have been carried out to evaluate the interplanar distance between backbone chains and to determine the more general crystallographic structure of the films. In addition, a few theoretical studies on rrP3ATs have been performed to determine the influence of the backbone tilting[13] and torsion[14] angle on the electronic properties. Nevertheless, there is still no consensus on the crystalline structure of rrP3ATs and furthermore, no theoretical studies are rigorously supporting a given crystalline structure, or are attempting to establish a relation between the crystalline structure and the electronic properties of the crystal. The present study aims to describe the variation in electronic properties of rrP3ATs from a random to a strongly organized polymer structure by performing first-principles density-functional theory (DFT) calculations on rrP3HT crystal. Results from the present work agree with most recent diffraction experiments and furthermore, the electronic properties and their relation with the crystalline structure of rrP3ATs is now clearly established. The present paper is built as follows: we first briefly describe the computational details in Sec. II. Then, we discuss the several crystal conformation considered in terms of π interactions and steric effects between the side chains. We finally describe the influence of structural organization within the rrP3HT crystal on its resulting electronic structure properties.

II. COMPUTATIONAL DETAILS

The structural and electronic calculations on the rrP3HT crystal were performed with the DFT method using the SIESTA (Ref. 15) software package. All DFT calculations were performed within local-density approximation (LDA) in conjunction with double-ζ polarized linear combination of atomic orbitals basis sets for carbon, hydrogen, and sulfur atoms. Norm-conserving Troullier-Martins pseudopotentials were generated with the ATOM software (in SIESTA package) and were thoroughly tested for accuracy and transferability, i.e., for their ability to replicate all-electron energy levels and wave functions in arbitrary environments. The pseudopotentials were built to reproduce the all-electron eigenvalues and excitation energies of multiple atomic configurations within 1 mRy error. The molecular geometries were fully optimized from the calculated forces and stresses following a quasi-Newton method using a Broyden-Fletcher-Goldfarb-Shanno procedure to update the Hessian matrix. The geometry optimization was pursued until the convergence criterion was

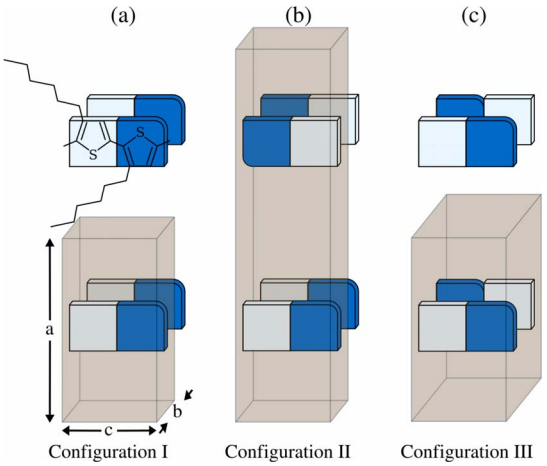

FIG. 1. (Color online) Representation of the polymer packing configuration (a) I, (b) II, and (c) III for a rrP3HT π-stacked crystal.

less than 10^{-4} Ry/Bohr for forces and less than 10^{-5} Ry for total energies.

In order to truly validate the choice of the pseudopotentials and the basis sets for the rrP3HT crystal system, we performed solid-state calculations on isolated polythiophene (PT) chains. The optimized molecular geometry and the band structure obtained for PT are very close to those reported in the literature,[16] where the maximum deviation in bond length is 1.6% and is 0.9% for angles. These differences are considered to be within the acceptable range for DFT-LDA calculations.[17] Although we will discuss this issue in more details below, we have deliberately chosen the LDA functional in the calculations for its proven ability to predict reasonable equilibrium distances in π-stacked systems,[18] and to correctly describe steric interactions between alkyl chains.[19] Finally, since we are discussing the stability of the different conformations in terms of relative energy, the known LDA underestimation of binding energy in weakly π-bound systems[20] should have a minimal impact on the conclusions of the present work.

III. RESULTS AND DISCUSSION

A. Geometry optimization

The orthorhombic unit cell of the rrP3HT crystal is characterized by vectors $\mathbf{a}=(a,0,0)$, $\mathbf{b}=(0,b,0)$, and $\mathbf{c}=(0,0,c)$ lying respectively in the alkyl side chains, the π-π stacking and the π-conjugated backbone directions (see Fig. 1). To limit the number of calculations, the value of c was optimized for an isolated chain, and then c was maintained constant for the remaining rrP3HT crystal configurations considered. Among the large amount of possible crystal configurations, the three most probable we have investigated are shown in Fig. 1.

The configuration I has an interplanar π-stacking separation of 5.0 Å, and is 425 meV/monomer more stable than the isolated chains. In contrast, configuration II, with an interplanar π-stacking separation of 4.5 Å, is unstable with respect to the isolated rrP3HT chains. Finally, configuration III shows an interplanar π-stacking separation of 3.42 Å,

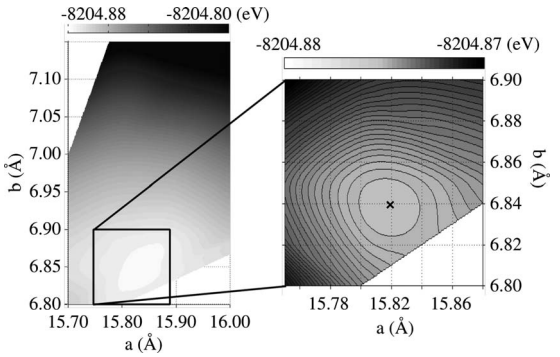

FIG. 2. Total energy for a unit cell in the configuration III as a function of the values of a and b. The minimum in total energy is indicated by a cross on the blow up graph.

and is 875 meV/monomer more stable than the isolated chains. Configuration III corresponds to the most stable packing structure investigated. At first glance, the variation in conformations stability can be associated to the different spatial distribution of the side chains. As opposed to what occurs in configurations I and II, the alkyl side chains in configuration III are evenly distributed, and minimize the steric repulsion between side chains. In configuration I, the alkyl side chains are closer in the **b** direction than in the **c** direction. In configuration II, although there is some interdigitation of alkyl side chains, their specific distributions are preventing an excessively compact packing of the polymer chains in the **b** direction. Furthermore, a combination of configuration II and III can be ruled out since the alkyl side chains of diagonal polymer chains (in the **ab** plan) would strongly overlap.

A systematic description of the structural properties of rrP3HT crystal is obtained by plotting the total energy for the unit cell in configuration III as a function of the structural parameters a and b as in Fig. 2. The total-energy standard deviation in Fig. 2 is less than 1 meV, and is invariantly obtained by repeating geometry optimization steps even when starting from different geometries. The expanded view of the main 2D map shows a relatively flat energy surface where the minimum indicated by the cross gives the equilibrium dimensions of the unit cell. The full color scale bar of the expanded view corresponds to a variation of 10 meV of the unit-cell total energy.

The molecular arrangement in configuration III is based on a model previously proposed by Prosa *et al.*[9,21] to describe a series of polymers including rrP3HT, poly(3-dodecylthiophene) and poly(3-octylthiophene) type-I crystal structure. Similar models were also proposed by Tashiro *et al.*[11] and by Brinkmann *et al.*[12] to describe the rrP3HT crystal structure. In Table I, we are comparing the experimental unit-cell parameters to the values obtained in our DFT calculations.

The calculated a and c values are within the incertitude of the more recent selected area electron-diffraction (SAED) measurement performed on single-crystal domains.[12] However, the calculated value for b (π-stacked interplanar distance) is ~12% lower than the experimental values. In order to explain this discrepancy, we first need to realize that the

TABLE I. Cell parameters of rrP3HT crystal.

Method	a (Å)	b (Å)	c (Å)	α (deg.)	β (deg.)	γ (deg.)
This work	15.82	6.84	7.83	90.0	90.0	90.0
XRD[a],[b]	16.80	7.66	7.70	90.0	90.0	90.0
XRD[c]	16.63	7.75	7.77	90.0	90.0	90.0
SAED[d]	16.00	7.80	7.80	90.0	90.0	93.5

[a]Reference 9.
[b]Reference 21.
[c]Reference 11.
[d]Reference 12.

stability of such branched polymer depends on two main type of interactions: (1) the π-dispersion interactions within the conjugated network and (2) the steric effect between alkyl side chains.

LDA or generalized gradient approximation (GGA) does not formally consider a treatment of dispersion energy involved in π-π interactions. Nevertheless, recent DFT-LDA calculations performed on graphite, an ideal system with nearly pure π-π interactions, give a slightly underestimated interlayer separation as opposed to the large overestimated value obtained with a GGA approach. The good performance of DFT-LDA in determining equilibrium distance is achieved despite the fact that the binding energy is underestimated at LDA level. This trend is even worse when a GGA approach is used since two graphene layers are found unbound with a B3LYP functional.[18,22] Nevertheless, since we are only comparing the relative DFT-LDA energies, an underestimation of dispersion energy has only a slight influence on the general trend found here.

Concerning the description of steric interactions between alkyl side chains, recent DFT calculations have shown that LDA gives a better description of equilibrium distances in the polyethylene crystal than GGA.[19] The LDA slightly underestimates the unit-cell parameters by 5% while GGA overestimates them by 18%. In summary, DFT-LDA method is still the best choice to determine the rrP3HT crystal structure and the stability of different conformations. Recent DFT methods that include van der Waals correction for taking account of long-range interactions give very promising results to describe weakly bounded systems but were mostly used in small molecular systems[23] and are not well tested on extended or periodic systems such as polymers.

We may alternatively explain the discrepancy in "*b*" by involving the fact that DFT computations do not consider the substrate on which the polymer is deposited, and which can significantly influence the orientation of crystal domains. For example, thin films of rrP3ATs deposited on highly oriented pyrolytic graphite (HOPG) form multiple microcrystalline domains that follow the threefold symmetry of the substrate.[24] In a more realistic explanation, we could consider that the folding of the polymer chains in the polycrystal are spanned over several microcrystal domains,[25] and introduce structural misalignment of the hexylthiophene units in the stacking direction as in Fig. 3. Experimentally, the most energetically favorable folding pattern could lead to a compromise between the two theoretically stable I and III configurations. The measured distance between two consecutive chains in the **b** direction are ranging from 3.83 to 3.90 Å, which is lying between the calculated 3.42 Å value for configuration III and 5.0 Å value for the configuration I crystal.

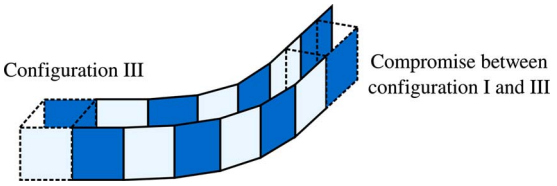

FIG. 3. (Color online) Representation of misalignment of hexylthiophene units that suggests a compromise between the I and III configurations.

The optimized structure obtained for the configuration III is schematized in Fig. 4 where we also define θ_1, θ_2, and θ_3 angles. The computed values of these angles are, respectively, 34.1°, 39.2°, and 6.9°. The calculated tilting angle for the alkyl side chains (50.1°) evaluated from θ_1 and θ_2 is nearly identical to the value (50.0°) proposed by Tashiro *et al.*[11] Such tilting angle allows a long 7.55 Å alkyl side chain to enter in the unit-cell dimensions without interdigitating. The θ_3 angle compares favorably with the predicted value (5.0°) for a type-I crystal model[9] and with the recent model proposed by Prosa *et al.*,[21] and is also consistent with recent DFT calculations showing that a rotation of the rrP3HT and similar conjugated polymers backbone is energetically favorable.[13]

B. Electronic structure

The band structure of rrP3HT crystal in configuration III illustrated in Fig. 5(a) shows important band dispersion in the interchain (stacking) direction from Γ to $X=(0,\pi/b,0)$ and a greater dispersion in the intrachain (backbone) direction from Γ to $X'=(0,0,\pi/c)$. This band structure exhibits strong similitudes with the band structure of PT crystal although PT usually forms a herringbone structure.[26] The presence of two polymer chains in the unit cell for the configuration III rrP3HT crystal doubles the number of bands, and the interchain interactions lead to a similar highest occupied

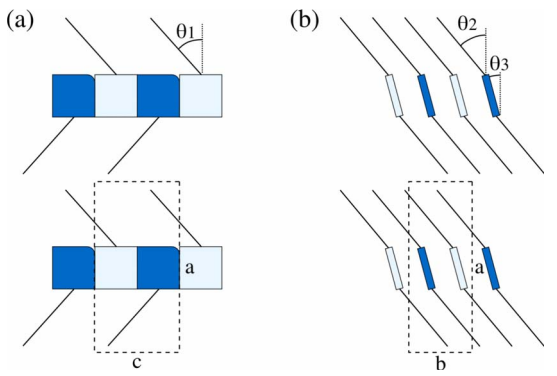

FIG. 4. (Color online) Representation of (a) a unit of rrP3HT and (b) of a rrP3HT crystal.

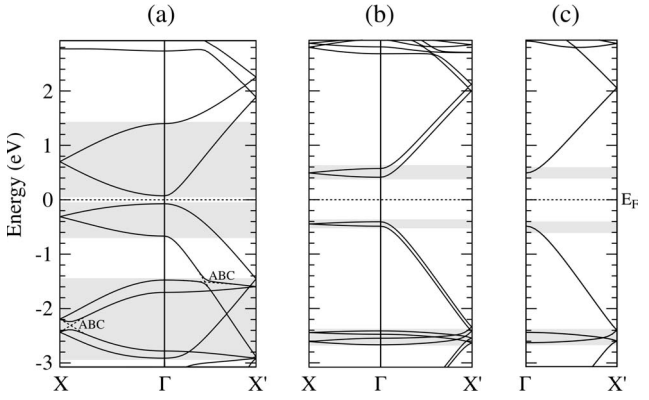

FIG. 5. Band structure of (a) rrP3HT crystal in configuration III, (b) rrP3HT crystal in configuration I, and (c) isolated rrP3HT chain.

molecular-orbital (HOMO) and lowest unoccupied molecular-orbital (LUMO) bands splitting at Γ. The band structure also displays numerous twofold band degeneracy at X and X' points, indicating the presence of two symmetry elements in the unit cell. The band degeneracy at X point is caused by a C_2 rotational symmetry while the other one at X' point is caused by a 2_1 screw-axis symmetry. Due to the important band dispersion, the band structure exhibits multiple band crossings and two avoided band crossings (ABC) below Fermi level (E_F). This behavior, also observed for the band structure of PT,[26] can be explained by the following. Bands avoid crossing each other when they have a same symmetry, i.e., when interactions between the bands are possible. The avoided band crossings identified by the shaded area in Fig. 5(a) involve bands with π symmetry. According to the noncrossing rule, other band crossings should also be avoided but since the symmetry elements within the unit cell folds the first Brillouin zone in two, the bands with similar symmetry appear to cross each other. This artificial band crossing could be clearly revealed by unfolding the band structure, a process we explain in more details below.

In order to appreciate the variation in band dispersion from a polymer packing to another, we also give the band structures of the rrP3HT crystal in configuration I in Fig. 5(b) and of the isolated rrP3HT chain in Fig. 5(c). This should help to clarify the complicated nature of the band structure of rrP3HT in the configuration III. Bands with similar symmetry properties with ABC near Γ point are also identified by shaded area. In order to enhance the similitude in terms of electronic properties between configuration I and III, the band structure for configuration I is given for a supercell made of two unit cells in the π-stacking direction. This supercell generates an artificial translation symmetry that folds the band structure over the first half of the Brillouin zone in the $\Gamma-X$ direction, and creates a twofold band degeneracy at this new zone edge.

The strong increase in the direct band gap and the important band dispersion decrease in the $\Gamma-X$ (π-stacking) direction observed from configuration III to configuration I are due to an increasing interchain spacing from 3.42 to 5.00 Å in the π-stacking direction. This last behavior contributes to decrease the magnitude of overlap between π-electron wave functions of individual chains. In addition, the decrease in band dispersion in configuration I lifts an ABC near −2.3 eV [see Fig. 5(b)].

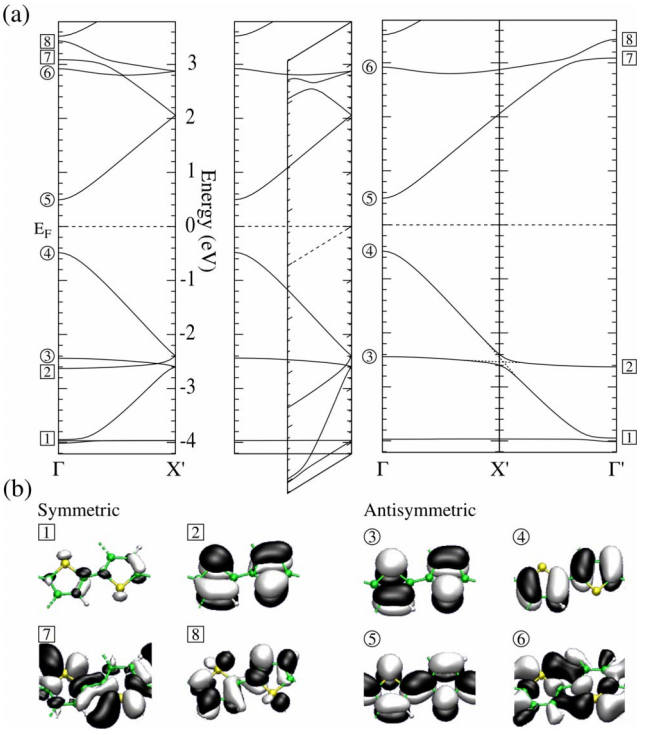

FIG. 6. (Color online) (a) Unfolding of the isolated rrP3HT chain band structure. The symmetric wave functions are unfolded at Γ′ and the antisymmetric wave functions are kept at Γ. (b) Wave functions identified on the band structure and classified following their symmetry.

The band gap and the band dispersion in the $\Gamma-X'$ (backbone) direction remain almost constant from configuration I to isolated rrP3HT chain. The band structures illustrated in Fig. 5 clearly reveal that π-π interactions are the most important interchain interactions that influence the dispersion along the polymer backbone along $\Gamma-X'$ direction. Surprisingly, the behavior of the bands in $\Gamma-X'$ direction is influenced by the presence of intrachain and interchain π-π interactions, while the presence of alkyl side chains interactions has a relatively weak influence on the band dispersion.

In order to exclude any ambiguities in the attribution of symmetry to a specific band, we performed the operation of band structure unfolding on the isolated rrP3HT chain around the 2_1 screw-axis symmetry that is illustrated in Fig. 6. The symmetric wave functions, with respect to the 2_1 symmetry, are completely unfolded toward Γ′ while the antisymmetric wave functions are maintained at Γ. The two π symmetry bands near −2.5 eV avoid crossing each other at the X' point, and the nature of the associated wave functions at the Γ and Γ′ points are drastically different. This expected behavior is more clearly identified by the dotted lines in the totally unfolded band structure of Fig. 6(a) and by the phase shift in the wave functions at the Brillouin-zone edge (Γ′) shown in Fig. 6(b). The presence of an ABC induces an apparent reduction in the total bandwidth of the HOMO band. Nevertheless, the nature of the top of the HOMO band

TABLE II. Influence of structural order on the band gap and on HOMO and LUMO bandwidths for the rrP3HT system (values in eV).

		HOMO		LUMO	
	Band gap	$\Gamma-X$	$\Gamma-X'$	$\Gamma-X$	$\Gamma-X'$
Isolated chain	0.97	0.00	2.15	0.00	2.37
π crystal	0.15	0.60	2.84	1.33	2.67
Difference	−0.82	0.60	0.69	1.33	0.30

which is the more relevant region for positive (hole) charge transport is unchanged, as the bottom of the LUMO band that is more associated to negative (electron) charge transport.

The band gaps and the HOMO and LUMO bandwidths determined from the unfolded band structures of rrP3HT in configuration III and from the isolated rrP3HT chain are displayed in Table II. The calculated band gaps should be considered as a lower limit since they are usually underestimated within the LDA limit, but the estimated HOMO and LUMO bandwidths in the $\Gamma-X'$ direction are similar to the values recently computed by Northrup.[13] The comparison of electronic properties for these two systems allows to identify the role of the structural order on the electronic properties of rrP3HT films in which the isolated rrP3HT chain represents a disordered and weakly coupled polymeric system. The most significant consequences of an improved structural order are definitely (1) a large decrease in the band gap (0.82 eV) and (2) an increase in HOMO and LUMO bandwidths in the $\Gamma-X$ and $\Gamma-X'$ directions. The increases in bandwidth are imputed to an improved interchain π-π coupling, facilitated by a cofacial structure such as in configuration III, which provoke an increasing overlap in the π-stacking direction between delocalized π-orbital centered on adjacent chains. Moreover, the nature of overlaps between the polymer chains in the organized crystal can be used to explain the difference in the behavior observed for HOMO and LUMO bandwidths. To visualize the nature of overlaps, the wave functions associated to the top of the HOMO band and the bottom of the LUMO band are reported in Fig. 7. A major difference between the HOMO and LUMO wave functions is that the HOMO is mostly localized on carbon atoms within the rrP3HT backbone, while a strong contribution in the LUMO originates from sulfur atoms that have electron lone pairs. Consequently, the formation of a π-stacked crystal improves

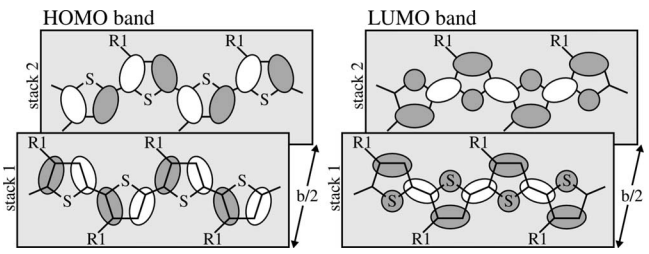

FIG. 7. HOMO and LUMO wave functions and their representation.

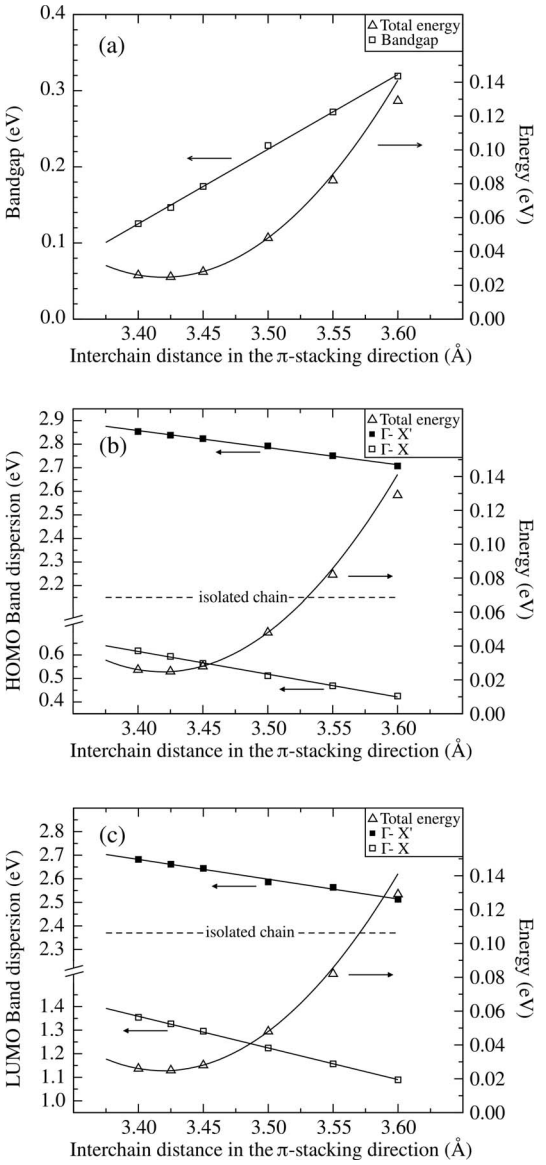

FIG. 8. Variation in the (a) gap, (b) HOMO, and (c) LUMO as a function of the interchain spacing.

the dispersion of HOMO states in both $\Gamma-X$ and $\Gamma-X'$ directions, while for the LUMO, the dispersion increases more significantly in the $\Gamma-X$ direction where the overlap between sulfur atoms is more readily established. A similar behavior of sulfur atoms on the HOMO and LUMO bands was previously observed for a one-dimensional (1D) stack of 4,4′-biphenyldithiol molecules.[27]

Finally, the influence of an external pressure on the band gap and the HOMO-LUMO bandwidths of the rrP3HT crystal in configuration III was considered. The pressure translates into a variation in the interchain spacing in both π-stacking and alkyl side chains directions. The variation in the electronic properties reported in Fig. 8 is essentially significant with a pressure applied in the π-stacking direction. Near the bottom of the potential-energy surface, a compression of the system causes a linear decrease in the band gap. Such band gap decrease has been reported for a pressure-induced insulator to semiconductor transition of a photocon-

ductor film made of strongly ordered liquid crystals.[28] The nature of the HOMO and LUMO bands can also be used to explain this behavior. The combination of individual HOMO wave function in the π-stacking direction leads to the formation of a π band that has an antibonding character (top HOMO band) near E_F, while the combination of LUMOs gives the π^* band that has a bonding character near the bottom of the band (bottom LUMO band). Consequently, a reduction in the π-stacking interchain spacing destabilizes the states located in the top of the π band (antibonding) while it stabilizes the states in the bottom of the π^* band (bonding). Such behavior was reported at several occasions for small molecule self-assemblies[27,29–32] but was not clearly identified for more complex oligomers and polymers.

Figure 8 also displays a linear dependence between the HOMO and LUMO bandwidths and the π-stacking interchain spacing. The rate of variation in the HOMO bandwidth is 0.97 eV/Å in the $\Gamma-X$ direction and is 0.72 eV Å in the $\Gamma-X'$ direction. For the LUMO, the rate is 1.34 eV/Å in the $\Gamma-X$ direction and is 0.84 eV/Å in the $\Gamma-X'$ direction. As expected, the interchain spacing in the π-stacking direction strongly influences the dispersion in the $\Gamma-X$ direction but also to a lesser degree, the dispersion in the $\Gamma-X'$ direction.

These important variations in bandwidth indicate a strong influence of the interchain spacing in the π-stacking direction on the electronic properties. Even a relatively weak reduction in the interchain distance by 0.05 Å near the equilibrium causes a variation of 33.8% in the band gap value, a variation of ~6.5% in the HOMO and LUMO bandwidths in the $\Gamma-X$ direction, and a variation of ~1.5% in the HOMO and LUMO bandwidths in the $\Gamma-X'$ direction. Considering a Young's modulus of 15 GPa in the π-stacking direction, such structural deformation of the unit cell would require an equivalent pressure of 1.6 kbar. This value, calculated from energy curve near its minimum, is similar to values reported in the literature.[33] Furthermore, the pressure is in the same range as the critical pressure of 2.2 kbar reported by Liu and Bard[28] that gives rise to an insulator to semiconductor transition.

IV. CONCLUSIONS

We have investigated the structural properties of rrP3HT crystal at the DFT-LDA level. The most energetically favorable configuration is a staggered structure that is 875 meV/monomer more stable than rrP3HT isolated chains. The computed band structure of the rrP3HT crystal displays band degeneracies at the Brillouin-zone edges X and X', which are results of two symmetry element in the unit cell. The importance of the π-π interactions in the rrP3HT crystal was described by computing the electronic properties of a disordered and a tightly packed rrP3HT crystal. The formation of the tightly packed crystal caused a significant decrease in the band gap by 0.82 eV, and an increase of 0.60 and 1.33 eV for the HOMO and LUMO dispersion, respectively. The magnitude of the π-π interactions were also studied as a function of interchain distance in the stacking direction. The important linear variations in the band gap and the HOMO-LUMO bandwidths as a function of the interchain distance were explained by the nature of the interactions between frontier orbitals within the molecular stacks.

Hence, the electronic properties engineering of the rrP3HT crystal appears possible through the creation of structural organization and by a modulation of interchain spacing in the π-stacking direction. This feature is of great importance for the creation of highly efficient organic solar cells that requires an optimization of the electronic properties of the materials used. Our results demonstrate the possibility of adjusting the electronic properties of a typical organic semiconductor used in solar cell through the careful control of its structural properties.

ACKNOWLEDGMENTS

We are grateful to RQCHP for providing computational resources and Arnaud Maillard is thankful to the Fonds Québécois de la Recherche sur la Nature et les Technologies (FQRNT) for financial support.

*arnaud.maillard@polymtl.ca
†alain.rochefort@polymtl.ca; http://nanostructures.phys.polymtl.ca

[1] T. A. Skotheim and J. Reynolds, *Conjugated Polymers: Processing and Applications* (CRC, USA, 2006).
[2] A. Dodabalapur, Mater. Today **9**, 24 (2006).
[3] A. Salleo, Mater. Today **10**, 38 (2007).
[4] J. H. Burroughes, D. D. C. Bradley, A. R. Brown, R. N. Marks, K. Mackay, R. H. Friend, P. L. Burns, and A. B. Holmes, Nature (London) **347**, 539 (1990).
[5] J. K. Borchardt, Mater. Today **7**, 42 (2004).
[6] N. Sariciftci, L. Smilowitz, A. Heeger, and F. Wudl, Science **258**, 1474 (1992).
[7] N. Sariciftci, Mater. Today **7**, 36 (2004).
[8] H. Sirringhaus *et al.*, Nature (London) **401**, 685 (1999).
[9] T. J. Prosa, M. J. Winokur, J. Moulton, P. Smith, and A. J. Heeger, Macromolecules **25**, 4364 (1992).
[10] S. Meille, V. Romita, T. Caronna, A. Lovinger, M. Catellani, and L. Belobrzeckaja, Macromolecules **30**, 7898 (1997).
[11] K. Tashiro, M. Kobayashi, T. Kawai, and K. Yoshino, Polymer **38**, 2867 (1997).
[12] M. Brinkmann and P. Rannou, Adv. Funct. Mater. **17**, 101 (2007).
[13] J. E. Northrup, Phys. Rev. B **76**, 245202 (2007).
[14] S. Darling, J. Phys. Chem. B **112**, 8891 (2008).
[15] J. M. Soler, E. Artacho, J. D. Gale, A. García, J. Junquera, P. Ordejón, and D. Sánchez-Portal, J. Phys.: Condens. Matter **14**, 2745 (2002).
[16] G. Brocks, J. Phys. Chem. **100**, 17327 (1996).
[17] G. Brocks and A. Tol, J. Phys. Chem. **100**, 1838 (1996).
[18] M. Hasegawa and K. Nishidate, Phys. Rev. B **70**, 205431 (2004).
[19] G. Barrera, S. Parker, A. Ramirez-Cuesta, and P. Mitchell, Mac-

romolecules **39**, 2683 (2006).
[20] LDA approach usually overestimated binding energy of systems that involve more covalent or short-range interactions.
[21] T. Prosa, M. Winokur, and R. McCullough, Macromolecules **29**, 3654 (1996).
[22] L. A. Girifalco and M. Hodak, Phys. Rev. B **65**, 125404 (2002).
[23] A. Dkhissi, J. M. Ducéré, R. Blossey, and C. Pouchan, J. Comput. Chem. (to be published).
[24] R. Payerne, M. Brun, P. Rannou, R. Baptist, and B. Grévin, Synth. Met. **146**, 311 (2004).
[25] B. Grévin, P. Rannou, R. Payerne, A. Pron, and J. Travers, Adv. Mater. **15**, 881 (2003).
[26] G. Bussi, A. Ruini, E. Molinari, M. Caldas, P. Puschnig, and C. Ambrosch-Draxl, Appl. Phys. Lett. **80**, 4118 (2002).
[27] A. Rochefort, R. Martel, and P. Avouris, Nano Lett. **2**, 877 (2002).
[28] C.-Y. Liu and A. J. Bard, Nature (London) **418**, 162 (2002).
[29] D. S. Seferos, S. A. Trammell, G. C. Bazan, and J. G. Kushmerick, Proc. Natl. Acad. Sci. U.S.A. **102**, 8821 (2005).
[30] W. T. Geng, M. Oda, J. Nara, H. Kondo, and T. Ohno, J. Phys. Chem. B **112**, 2795 (2008).
[31] A. Rochefort and P. Boyer, Appl. Phys. Lett. **89**, 092115 (2006).
[32] A. Rochefort, P. Boyer, and B. Nacer, Org. Electron. **8**, 1 (2007).
[33] X. Wang and X. Feng, J. Mater. Sci. Lett. **21**, 715 (2002).